







RESEARCH ARTICLE

Brain olfactory-related atrophy in isolated rapid eye movement sleep behavior disorder

Kyung Ah Woo^{1,*} , Heejung Kim^{2,3,*}, Eun Jin Yoon^{2,4}, Jung Hwan Shin⁵ , Hyunwoo Nam¹ , Beomseok Jeon⁵ , Yu Kyeong Kim²  & Jee-Young Lee¹ 

¹Department of Neurology, Seoul Metropolitan Government–Seoul National University Boramae Medical Center, Seoul National University College of Medicine, Seoul, Republic of Korea

²Department of Nuclear Medicine, Seoul Metropolitan Government–Seoul National University Boramae Medical Center, Seoul National University College of Medicine, Seoul, Republic of Korea

³Institute of Radiation Medicine, Medical Research Center, Seoul National University, Seoul, Republic of Korea

⁴Memory Network Medical Research Center, Seoul National University, Seoul, Republic of Korea

⁵Department of Neurology, Seoul National University Hospital, Seoul National University College of Medicine, Seoul, Republic of Korea

Correspondence

Yu Kyeong Kim, Department of Nuclear Medicine, Seoul Metropolitan Government–Seoul National University Boramae Medical Center, Seoul National University College of Medicine, Seoul, Republic of Korea. Tel: 82-2-870-2581; Fax: 82-2-870-3863; E-mail: yk3181@snu.ac.kr

Jee-Young Lee, Department of Neurology, Seoul Metropolitan Government–Seoul National University Boramae Medical Center, Seoul National University College of Medicine, Seoul, Republic of Korea. Tel: 82-2-870-2476; Fax: 82-2-831-2826; E-mail: wieber04@snu.ac.kr

Received: 14 April 2023; Revised: 10 August 2023; Accepted: 9 September 2023

Annals of Clinical and Translational Neurology 2023; 10(12): 2192–2207

doi: 10.1002/acn3.51905

*These authors contributed equally to this work.

Abstract

Objective: To investigate structural and functional connectivity changes in brain olfactory-related structures in a longitudinal prospective cohort of isolated REM sleep behavior disorder (iRBD) and their clinical correlations, longitudinal evolution, and predictive values for phenoconversion to overt synucleinopathies, especially Lewy body diseases. **Methods:** The cohort included polysomnography-confirmed iRBD patients and controls. Participants underwent baseline assessments including olfactory tests, neuropsychological evaluations, the Movement Disorders Society–Unified Parkinson's Disease Rating Scale, 3T brain MRI, and ¹⁸F-FP-CIT PET scans. Voxel-based morphometry (VBM) was performed to identify regions of atrophy in iRBD, and volumes of relevant olfactory-related regions of interest (ROI) were estimated. Subgroups of patients underwent repeated volumetric MRI and resting-state functional MRI (fMRI) scans after four years. **Results:** A total of 51 iRBD patients were included, with 20 of them converting to synucleinopathy (mean time to conversion 3.08 years). Baseline VBM analysis revealed atrophy in the right olfactory cortex and gyrus rectus in iRBD. Subsequent ROI comparisons with controls showed atrophy in the amygdala. These olfactory-related atrophies tended to be associated with worse depression, anxiety, and urinary problems in iRBD. Amygdala ¹⁸F-FP-CIT uptake tended to be reduced in iRBD patients with hyposmia (nonsignificant after multiple comparison correction) and correlated with urinary problems. Resting-state fMRI of 23 patients and 32 controls revealed multiple clusters with aberrant olfactory-related functional connectivity. Hypoconnectivity between the putamen and olfactory cortex was associated with mild parkinsonian signs in iRBD. Longitudinal analysis of volumetric volumetric MRI in 22 iRBD patients demonstrated four-year progression of olfactory-related atrophy. Cox regression analysis revealed that this atrophy significantly predicted phenoconversion. **Interpretation:** Progressive atrophy of central olfactory structures may be a potential indicator of Lewy body disease progression in iRBD.

Background

The olfactory structure is recognized as one of the earliest locations where Lewy body pathology develops in the

brain. According to the Braak staging system, Lewy pathology is first observed in the olfactory bulb and dorsal motor nucleus of the vagus nerve, followed by the amygdala and pons, before affecting the dopaminergic

neurons of the substantia nigra.¹ This corresponds to the clinical observation that olfactory dysfunction is commonly observed in the two Lewy body diseases (LBDs), that is, Parkinson's disease (PD) and dementia with Lewy bodies (DLB).^{2–4} Clinically, olfactory dysfunction is present in 80%–90% of the patients at the time of PD diagnosis.² Postmortem studies in PD have revealed extensive Lewy pathology throughout the olfactory system, including the amygdala, olfactory tubercle, anterior olfactory nucleus, piriform, and entorhinal cortices.^{5,6}

Olfactory dysfunction manifests several years before the onset of motor parkinsonism^{7,8} which may represent an early pathophysiological process in the preclinical stages of LBDs. In isolated rapid eye movement (REM) sleep behavior disorder (iRBD), a strong prodromal marker of PD,^{9–11} olfactory impairment is associated with an increased risk of phenoconversion within a few years.^{7,12} Microstructural alterations in brain olfactory-related structures have been observed in diffusion tensor imaging (DTI) studies of iRBD patients.¹³ Notably, experimental studies in rodent models have also indicated that the olfactory bulb and related structures could be possible sites for the induction of brain Lewy pathology.^{14–16} Injecting α -synuclein preformed fibrils into olfactory bulbs of wild-type mice results in sequential progression of Lewy-like pathology through the olfactory network, accompanied by clinical hyposmia.^{14,17} Based on these findings, we hypothesized that structural alterations and functional connectivity changes in olfactory-related brain regions may exist and progress in iRBD, and that they are associated with prodromal parkinsonian signs and an increased risk of phenoconversion.

To investigate this hypothesis, we enrolled patients with iRBD and conducted baseline assessments of prodromal parkinsonian symptoms, olfactory function, and cognition. Additionally, we performed volumetric, dopaminergic, and resting-state functional imaging studies. The patients were prospectively followed to monitor phenoconversion. Subgroups of patients underwent repeated structural and resting-state functional MRI (fMRI) at 4-year follow-up visits. We assessed the predictive value of baseline atrophy in olfactory-related structures for phenoconversion in iRBD patients and examined the potential longitudinal progression of this atrophy.

Methods

Study participants

We consecutively recruited a prospective cohort of iRBD patients aged 50 to 80 from the movement disorders clinic of Seoul National University Boramae Medical Center (SNUBMC) between 2013 and 2015, as previously described.¹⁸ A second cohort of iRBD patients who met

the same criteria and were recruited since 2017 was also included. The diagnosis of iRBD was based on the International Classification of Sleep Disorders, second Edition, and confirmed through video polysomnography.

None of the patients exhibited parkinsonism or dementia at the time of enrollment. Patients presenting any additional core clinical feature suggestive of DLB, other than RBD, were excluded.¹⁹ Patients with depression or other psychiatric disorders, severe obstructive sleep apnea (OSA), or any structural or vascular brain damage, including moderate to severe small vessel disease, were also excluded. However, mild and/or treated OSA was not considered an exclusion criterion if iRBD was confirmed in video polysomnography.

Patients underwent baseline clinical evaluations, 3T volumetric MRI, and ¹⁸F-FP-CIT positron emission tomography (PET) scans upon enrollment. For patients enrolled between 2013 and 2015, a repeat 3T volumetric MRI was conducted 4 years after enrollment for those who provided their consent. Resting-state fMRI scans were acquired at both enrollment and the 4-year follow-up period with additional consent. Healthy control data from our center, including 3T volumetric MRI, ¹⁸F-FP-CIT PET, and resting-state fMRI scans, were utilized for comparison as previously described.^{20,21}

Baseline clinical evaluation

In patients with iRBD, prodromal motor and nonmotor symptoms were assessed at enrollment using the Movement Disorders Society Revised–Unified Parkinson's Disease Rating Scale (MDS-UPDRS). Mild parkinsonian signs (MPS) were defined as a motor score on the MDS-UPDRS > 6, excluding action and postural tremor.^{9,22,23} Olfactory function was evaluated using either the Butanol Threshold Test (BTT) or the Korean Version of Sniffin' Sticks (KVSS) test (YOF test, Kimex Co., Suwon, Korea), which assesses olfactory threshold, discrimination, and identification using eight universal and four Korean culture-friendly odorants.²⁴ Hyposmia or anosmia was defined as a BTT score below 6 or a total KVSS score below 22. Cognition was assessed through a comprehensive neuropsychological test, as previously described,²⁵ and the results were presented as z-scores adjusted for age and years of education. Mild cognitive impairment (MCI) was defined according to level II of the MDS criteria.²⁶

Image acquisition and preprocessing

MRI acquisition and volumetric analysis

Participants underwent 3T MRI scan (Achieva, Philips Medical Systems, Best, The Netherlands) as previously described.²⁰ The volumetric T1 images were obtained

using the following acquisition parameters: a repetition time (TR) of 9.9 ms and an echo time (TE) of 4.6 ms, with a flip angle of 8.0°. The images had a slice thickness of 1 mm and an image matrix size of $224 \times 224 \times 180$. The voxel size was $0.98 \times 0.98 \times 1 \text{ mm}^3$. VBM was performed using CAT12 toolbox in SPM12 (<http://www.fil.ion.ucl.ac.uk/spm/software/spm12>). The detailed protocol is provided in the [Supporting Information](#). ROI volumes for amygdala, olfactory cortex, gyrus rectus, putamen, caudate, and pallidum were extracted using the Automated Anatomical Labelling (AAL) template.^{27,28}

Functional connectivity

Resting-state fMRI scans were obtained using a T2*-weighted echo-planar image (EPI) sequence (180 volumes, TR = 2700 ms, TE = 35 ms, voxel size = $1.53 \times 1.53 \times 4 \text{ mm}$, field of view (FOV) = $220 \times 220 \text{ mm}$, 35 slices, flip angle = 90°, and slice thickness = 4 mm). Participants were instructed to rest with eyes open during the scan. The data were analyzed using DPARSF (<http://www.restfmri.net/forum/dparsf>) based on MATLAB. The detailed protocol is provided in the [Supporting Information](#). The olfactory cortex, gyrus rectus, and amygdala based on the AAL template were defined as seed ROIs. The correlation coefficients were converted to *z* values using Fisher's *r*-to-*z* transformation.

Statistical analysis of image data

To evaluate differences between the iRBD and controls in GM volume, two-sample *t*-test with age and total intracranial volume as nuisance covariates was performed. Permutation-based inferences (5000 permutations) with threshold-free cluster enhancement (TFCE) was used to correct for multiple comparisons, providing strict control while improving replicability. A *p* < 0.01 threshold was considered significant. For seed-based functional connectivity analysis, two-sample *t*-test was performed to evaluate differences between iRBD and controls, with age as nuisance covariate. Significant differences in functional connectivity were reported using criteria of Gaussian random field (GRF) theory correction for multiple comparisons (two-tailed, voxel-level *p* value < 0.01, cluster-level *p* value < 0.05). For exploratory analysis of baseline and longitudinal fMRI scans in the subgroup with follow-up fMRI scans, the criteria of voxel-level *p* value < 0.05 and cluster-level *p* value < 0.05 were applied.

¹⁸F-FP-CIT PET analysis

A 10-min emission PET scan was performed 2 h after ¹⁸F-FP-CIT (185 MBq) intravenous injection (Philips

Gemini TF-64 PET/CT scanner, Philips Healthcare, Best, the Netherlands) as previously described.^{18,20} ROIs of bilateral amygdala, caudate nuclei, anterior and posterior putamen, and cerebellum (reference region) were automatically delineated with FSL version 5.0.2.

Follow-up and phenoconversion to overt synucleinopathy

Patients with iRBD were regularly followed up in-person by a movement disorders specialist (J-Y Lee) every 3–4 months to monitor phenoconversion. Parkinsonism was defined as presence of bradykinesia plus either rigidity or rest tremor. PD diagnosis was made with the MDS clinical diagnostic criteria for PD.²⁹ All multiple system atrophy (MSA) converters met the 2008 criteria for probable MSA. DLB diagnosis was based on the 2017 consensus criteria.¹⁹ Those who developed cognitive decline confirmed on follow-up neuropsychological testing, along with any additional core features of DLB such as cognitive fluctuations or vivid spontaneous visual hallucinations, were also defined as DLB converters even if there was no overt impairment in activities of daily living (ADL). All iRBD patients who developed PD, DLB, or MSA during follow-up were classified as phenoconverters in the statistical analysis.

Statistical analysis

Data are presented as mean (standard deviation; SD) unless otherwise specified. The average volume and standardized uptake value ratio (SUVr) of each ROI in the bilateral hemispheres are presented. Shapiro–Wilk test was used to assess the normality of the data. For comparisons between two independent groups, the independent *t*-test or Mann–Whitney test was employed. Analysis of covariance (ANCOVA) was used for comparisons involving two or more groups while controlling for age and sex. Fisher's exact test or chi-square test was used for categorical variables. The Jonckheere–Terpstra test was employed to examine for any increasing or decreasing trend of imaging variables with respect to the severity of nonmotor symptom categories evaluated by the MDS-UPDRS-I ordinal scale. To assess the correlation between continuous variables, Pearson's partial correlation analysis was conducted controlling for age and sex. Time-dependent changes in ROI volumes within subgroups were compared with repeated measures ANOVA (RM-ANOVA), with phenoconversion or baseline olfactory status as between-subject factors and time as the within-subject factor.

Kaplan–Meier plots were utilized to display the cumulative event-free survival, with censoring time defined as the time until phenoconversion for converters and the time

until last in-person assessment for nonconverters. The log-rank test was employed to compare the Kaplan–Meier plots between subgroups. Cox proportional hazards analysis was performed to calculate hazard ratios (HR) for each clinical, radiological, and ^{18}F -FP-CIT PET variable, adjusting for age and sex. Continuous variables in the radiological and ^{18}F -FP-CIT PET data were categorized into binary variables using a cutoff point determined as [(mean value of healthy controls) – (1 or 2SD)].

Statistical analyses were conducted using SPSS 23.0 (SPSS Inc, Chicago IL) and R software, version 3.6.0. (R project for Statistical Computing) with a significance level set at 0.05. Multiple comparisons were adjusted with the false discovery rate (FDR) method with a significance level of 0.05 for FDR control,³⁰ and Bonferroni correction was used for the post hoc analysis of ANCOVA in three groups.

Results

Clinical characteristics of the participants

A total of 51 patients with iRBD were included in the study. The clinical and demographic characteristics of the patients are presented in Table 1. All patients underwent baseline 3T volumetric MRI, and 48 also underwent ^{18}F -FP-CIT PET scans at enrollment. Baseline resting-state fMRI was performed in 25 patients who provided additional consent for the scan, and 23 were included in the analysis due to motion artifact in the two excluded patients. No significant demographic differences were observed between the iRBD patients and healthy controls for ^{18}F -FP-CIT PET (Table 2) or resting-state fMRI ($p > 0.05$ for age and sex). In the subsequent analyses, the difference in sex distribution between the iRBD patients and controls for volumetric MRI was controlled for.

After 4 years of enrollment, follow-up 3T volumetric MRI was performed on 22 patients enrolled between 2013 and 2015. Seven patients were excluded from the follow-up imaging due to reasons such as death, head trauma, refusal of follow-up imaging, or loss to follow-up. Similarly, among the 23 patients included in the baseline resting-state fMRI analysis, 4-year follow-up fMRI scans were obtained in 17 patients, and 16 were included in the analysis excluding one with motion artifacts on the 4-year scan (Fig. S1).

Baseline changes in olfactory-related structures in iRBD

We initially conducted whole-brain VBM to identify areas of atrophy in iRBD patients compared to controls. Subsequently, we estimated the volumes of associated ROIs using an objective atlas.

Table 1. Baseline clinical characteristics of the study participants.

	iRBD
<i>n</i>	51
Age, years	70.24 (5.985)
Sex, M/F	29/22
MDS-UPDRS-III score	7.245 (5.463)
MPS	20 (39.22%)
Hyposmia	31 (60.78%)
Constipation (max 4 ^a)	0.784 (0.945)
Urinary problems (max 4 ^b)	1.020 (1.029)
MMSE score	26.66 (2.925)
NPT, z-scores	
DST	0.102 (0.886)
TMT.A	−0.662 (2.643)
CWST	−0.750 (1.212)
BNT	−0.187 (1.183)
RCFT	−1.433 (1.505)
SVLT.imm	−0.306 (0.962)
SVLT.delayed	−0.678 (1.128)
SVLT.recog	−0.239 (1.142)
COWAT.s	−0.291 (1.056)
COWAT.p	−0.692 (0.857)
TMT.B	−1.792 (3.043)
Follow-up, years	4.110 (2.339)
Phenoconversion	
Total converters	20 (39.22%)
PD	11 (21.57%)
DLB	7 (13.73%)
MSA	2 (3.92%)

Detailed information on the control groups, that is, controls for MRI and PET, is provided in Table 2.

BNT, Boston Naming Test; COWAT, Controlled Oral Word Association Test; CWST, Color Word Stroop Test; DLB, Dementia with Lewy Bodies; DST, Digit Span Test; MMSE, Mini-Mental Status Examination; MPS, mild parkinsonian sign; MSA, Multiple System Atrophy; NPT, neuropsychological test; PD, Parkinson's disease; RCFT, Rey Complex Figure Test; SVLT, Seoul Verbal Learning Test; TMT, Trail Making test.

^aMDS-UPDRS item I.11 score.

^bMDS-UPDRS item I.10 score.

Whole-brain VBM analysis at baseline

Significant differences in gray matter volume were found between iRBD patients and healthy controls (Fig. 1 and Table S1). Compared to controls, iRBD patients exhibited reduced gray matter volume in the right olfactory cortex, right gyrus rectus, and left postcentral gyrus.

Baseline olfactory-related ROI volumes, dopaminergic denervation, and clinical correlations

Based on the VBM findings of olfactory cortical and gyrus rectus atrophy, we selected olfactory-related ROIs based on the AAL atlas, including the olfactory cortex, gyrus

Table 2. Comparison of baseline brain ROI volumes based on AAL templates and ^{18}F -FP-CIT SUVR of the iRBD patients and healthy controls.

ROI volumes (cm^3)			
	iRBD	Control-MRI	FDR-adjusted p value
<i>n</i>	51	39	
Age	70.24 (5.985)	69.51 (5.124)	0.548
Sex, M/F	29/22	11/28	0.007
Olfactory cortex	1.020 (0.129)	1.085 (0.123)	0.001
Gyrus rectus	2.168 (0.253)	2.347 (0.301)	< 0.001
Amygdala	1.110 (0.124)	1.155 (0.125)	0.001
Putamen	3.805 (0.391)	4.013 (0.463)	0.003
Caudate	2.792 (0.372)	2.891 (0.482)	0.244
Pallidum	0.462 (0.118)	0.479 (0.106)	0.263

^{18}F -FP-CIT SUVR			
	iRBD-DAT ^a	Control-PET	FDR-adjusted p value
<i>n</i>	48	19	
Age	70.15 (6.035)	69.42 (4.706)	0.640
Sex, M/F	28/20	7/12	0.112
Amygdala	0.831 (0.235)	0.916 (0.123)	0.180
Anterior putamen	4.792 (1.632)	5.783 (0.864)	0.098
Posterior putamen	4.078 (1.634)	5.045 (0.834)	0.098
Caudate	3.706 (1.340)	4.389 (0.857)	0.180
Pallidum	2.163 (0.616)	2.575 (0.467)	0.098

The analyses are controlled for age and sex, and FDR-adjusted p values are provided for multiple comparisons of ROIs. Data are presented as mean (standard deviation; SD) unless otherwise specified. FDR, false discovery rate; ROI, region of interest; SUVR, standardized uptake value ratio.

^aRepresents the subgroup of patients with iRBD that underwent baseline ^{18}F -FP-CIT PET.

rectus, and amygdala, and estimated their volumes. The volumes of these three ROIs were all significantly reduced in the iRBD group compared to controls, controlling for age and sex ($p_{\text{FDR}} < 0.05$, Table 2).

The trend of olfactory-related ROI volumes and amygdala dopaminergic denervation was analyzed based on the severity of nonmotor features at baseline (Fig. 2). The volume of the rectal gyrus and the FP-CIT SUVR of the amygdala significantly decreased with higher severity of urinary problems (p for trend = 0.024 and 0.004; $p_{\text{FDR}} < 0.05$). Olfactory cortex volume showed a decreasing trend with increasing anxiety and depression severity, but lost statistical significance after multiple comparison correction across ROIs (p for trend = 0.049 and 0.023; $p_{\text{FDR}} > 0.05$).

Group comparisons between healthy controls and subgroups of iRBD patients stratified by MPS or olfactory

dysfunction, controlling for age and sex, revealed consistent reductions in the volumes of the amygdala, olfactory cortex, and gyrus rectus in all iRBD subgroups (Bonferroni-corrected $p < 0.05$, Fig. S2) compared to controls. However, no significant differences were found between iRBD patients with and without MPS or between iRBD patients with and without olfactory dysfunction. The amygdala ^{18}F -FP-CIT SUVR tended to be reduced in iRBD patients with olfactory dysfunction compared to controls (uncorrected $p = 0.049$), although this did not reach statistical significance after multiple comparison correction.

Clinical outcome of the cohort and survival analysis

Out of the 51 patients with iRBD, a total of 20 individuals (11 PD, 2 MSA, 7 DLB) converted to overt synucleinopathy during a mean follow-up duration of 4.11 years (SD 2.339). The average time to conversion from enrollment was 3.08 years (SD 1.88, range 1–7.5 years). The Kaplan–Meier curve of the entire cohort is shown in Fig. 3A.

Kaplan–Meier curves stratified by baseline olfactory-related ROI atrophy are shown in Fig. 3B–D. The cutoff values were set 1 SD below the mean of healthy controls (HC) for each ROI volume (HC–1SD). Subgroups of iRBD patients with baseline atrophy in the gyrus rectus (log-rank test, $p = 9\text{e}–04$) and amygdala ($p = 0.03$) had significantly higher rates of phenoconversion than those without baseline atrophy.

In Cox proportional hazards analyses, controlling for age and sex, the presence of baseline olfactory-related atrophy (below HC–1SD) in the olfactory cortex (HR 3.90, 95% CI 1.35–11.20), the gyrus rectus (HR 4.52, 95% CI 1.69–12.11), and the amygdala (HR 4.12, 95% CI 1.33–12.80) significantly predicted phenoconversion, as did baseline hyposmia and reduced putaminal ^{18}F -FP-CIT SUVR (Table S2). Additionally, in a combined Cox analysis, olfactory cortical atrophy and hyposmia were independently associated with an increased risk of phenoconversion (Fig. S3).

Among the phenoconverters, there were no statistically significant differences in baseline olfactory-related ROI volumes or amygdala ^{18}F -FP-CIT SUVR between PD and DLB phenoconverters.

Survival analysis excluding MSA converters

The clinical significance of olfactory dysfunction in MSA remains controversial. According to the recently revised MDS criteria, unexplained anosmia is an exclusion criterion for clinically established and possible MSA.³¹ We

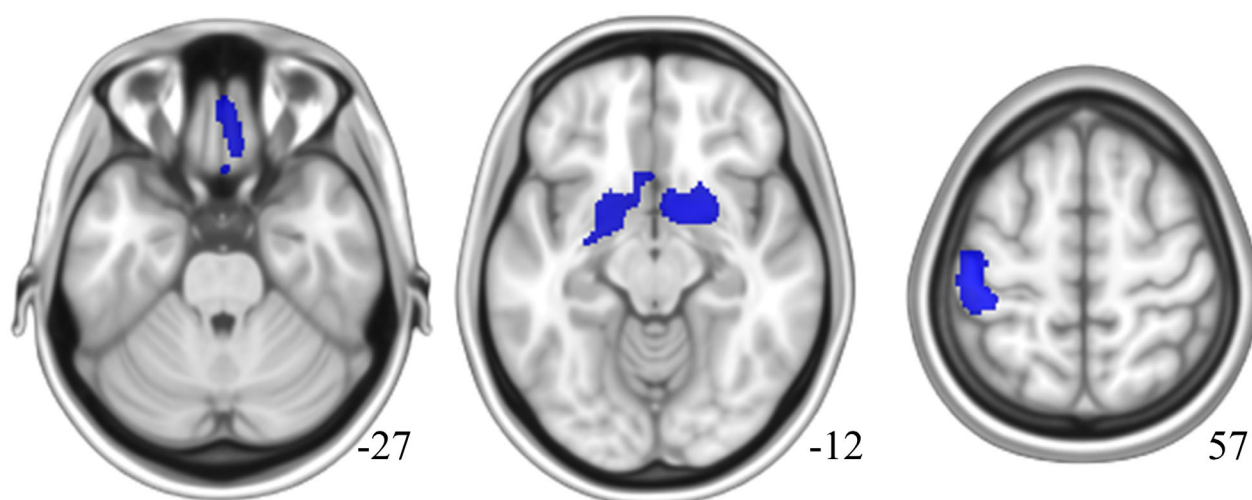


Figure 1. Baseline voxel-based morphometry (VBM) results comparing 51 patients with iRBD and 39 healthy controls. VBM was performed using the CAT12 toolbox in SPM12. The contrast map displays brain regions demonstrating significant changes in gray matter volume in patients with iRBD compared to controls, including the postcentral gyrus, olfactory cortex, and gyrus rectus. A two-sample *t*-test was conducted, and corrections for multiple comparisons were performed using permutation-based inferences (5000 permutations) with threshold-free cluster enhancement (TFCE). The significance threshold was set at $p < 0.01$, family-wise error correction (FWE) corrected.

summarized the profiles of the two iRBD patients who converted to MSA (refer to the [Supporting Information](#)) and conducted additional survival analyses excluding these MSA converters to evaluate the predictive power of olfactory-related atrophy exclusively for LBDs.

The Kaplan–Meier curves of the cohort of 49 iRBD patients, excluding the two MSA converters, are shown in Fig. S4. Subgroups with baseline atrophy in the gyrus rectus (log-rank test, $p = 0.0013$) and amygdala ($p = 0.016$) still demonstrated significantly higher rates of phenocconversion compared to those without baseline atrophy. The predictive value of each olfactory-related ROI atrophy remained significant ($p < 0.05$), with higher HR for each ROI compared to the analysis that included MSA converters (olfactory cortex HR 3.95, 95% CI 1.35–11.54; gyrus rectus HR 4.79, 95% CI 1.72–13.33; amygdala HR 4.15, 95% CI 1.32–13.04; Table S3).

Four-year progression of olfactory-related atrophy in patients with iRBD

Among the 22 iRBD patients who underwent repeated volumetric MRI after 4 years, there was progressive atrophy observed in the olfactory cortex, gyrus rectus, and amygdala ($p < 0.001$), with average volume reductions of 6.85%, 9.61%, and 5.67%, respectively (Fig. 4A–C). Patients with baseline olfactory dysfunction showed greater atrophy in amygdala compared to normosmic patients (7.93% vs. 3.89%, time*group $p = 0.014$; Fig. 4D). However, there were no significant differences

between the hyposmia/anosmia and normosmia groups in the degree of volume reduction of the olfactory cortex or gyrus rectus (Fig. 4E,F).

Out of the 22 patients, nine developed overt synucleinopathy, all of which were LBDs (3 PD, 6 DLB), with an average time to conversion of 4.41 years (SD 2.02). The converters showed a faster progression of amygdala atrophy compared to nonconverters (average volume reduction 8.31% vs. 4.03%, time*group $p = 0.019$; Fig. 4G). The converters also demonstrated significant atrophy in the gyrus rectus (group $p = 0.015$) and a trend of atrophy in the olfactory cortex (group $p = 0.065$) compared to the nonconverters, but the degree of atrophy progression over the 4 years did not differ significantly between converters and nonconverters in both areas (Fig. 4H,I).

Aberrant olfactory-related functional connectivity and its longitudinal changes in patients with iRBD

Baseline olfactory-related functional connectivity networks in iRBD and their clinical correlations

A group comparison of seed-to-voxel resting-state fMRI networks was conducted between iRBD and healthy controls using bilateral olfactory-related seed ROIs (Fig. 5). In the iRBD group, gray matter regions with reduced connectivity with the right olfactory cortex included a cluster involving the contralateral putamen and superior orbitofrontal cortex, another cluster involving the

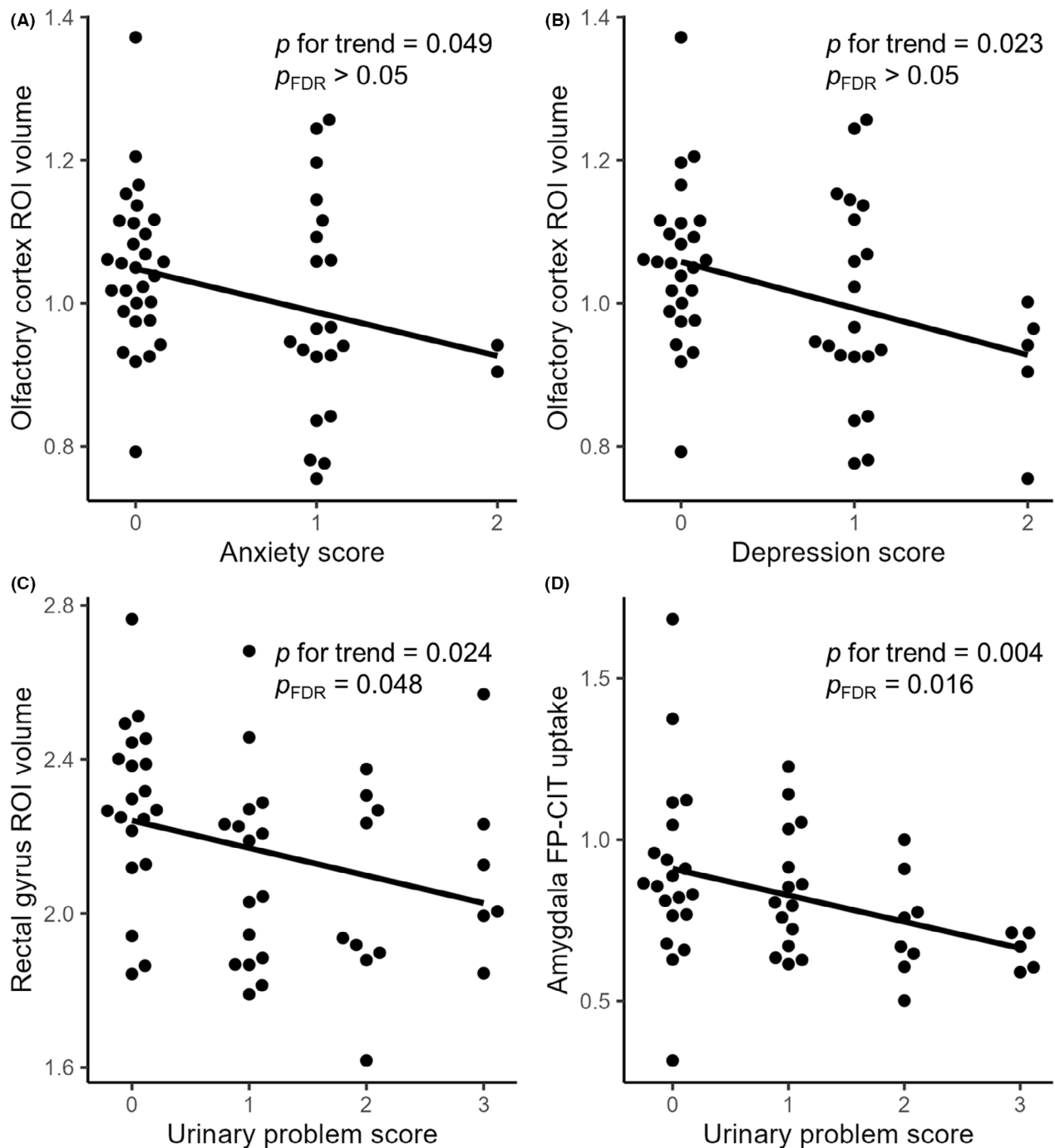


Figure 2. (A–D) Trends in baseline volumes of olfactory-related regions of interest (ROIs; A–C) and amygdala ^{18}F -FP-CIT SUVR (D) based on nonmotor symptom severity in patients with iRBD. To analyze these trends, a nonparametric Jonckheere–Terpstra test was employed. FDR-adjusted p values for multiple comparisons are also provided. FDR, false discovery rate; ROI, region of interest.

contralateral middle cingulate cortex and paracentral lobule, and a third cluster involving the ipsilateral superior orbitofrontal cortex (Fig. 5A). Hypoconnectivities with the left olfactory cortex and with left amygdala

were detected in left precentral gyrus (Fig. 5B,C). Additionally, increased functional connectivity with the left gyrus rectus was detected in the right middle occipital and temporal cortices (Fig. 5D). A detailed information

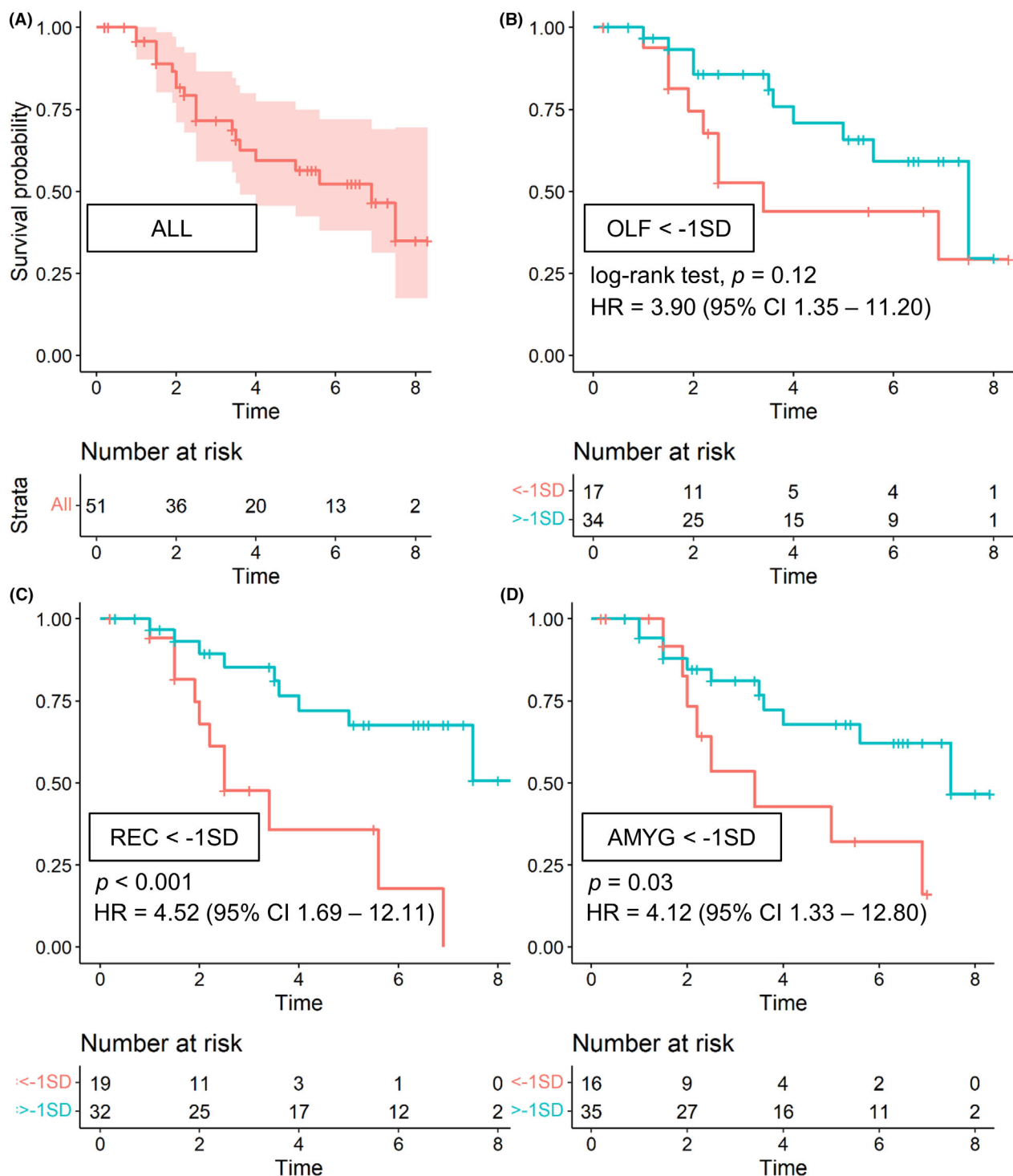


Figure 3. Kaplan–Meier curves showing disease-free survival in patients with iRBD. (A) Cumulative survival plot of all 51 patients with iRBD. (B–D) Comparison of disease-free survival stratified by the presence of baseline atrophy in the olfactory cortex (OLF; B), gyrus rectus (REC; C), and amygdala (AMYG; D) using the log-rank test. The cutoff values for atrophy were set 1 standard deviation (SD) below the mean of healthy controls ($HC_{mean} - 1SD$). Hazard ratios of phenoconversion for each ROI atrophy were calculated by Cox regression. Time presented as years. CI, confidence interval; HR, hazard ratio.

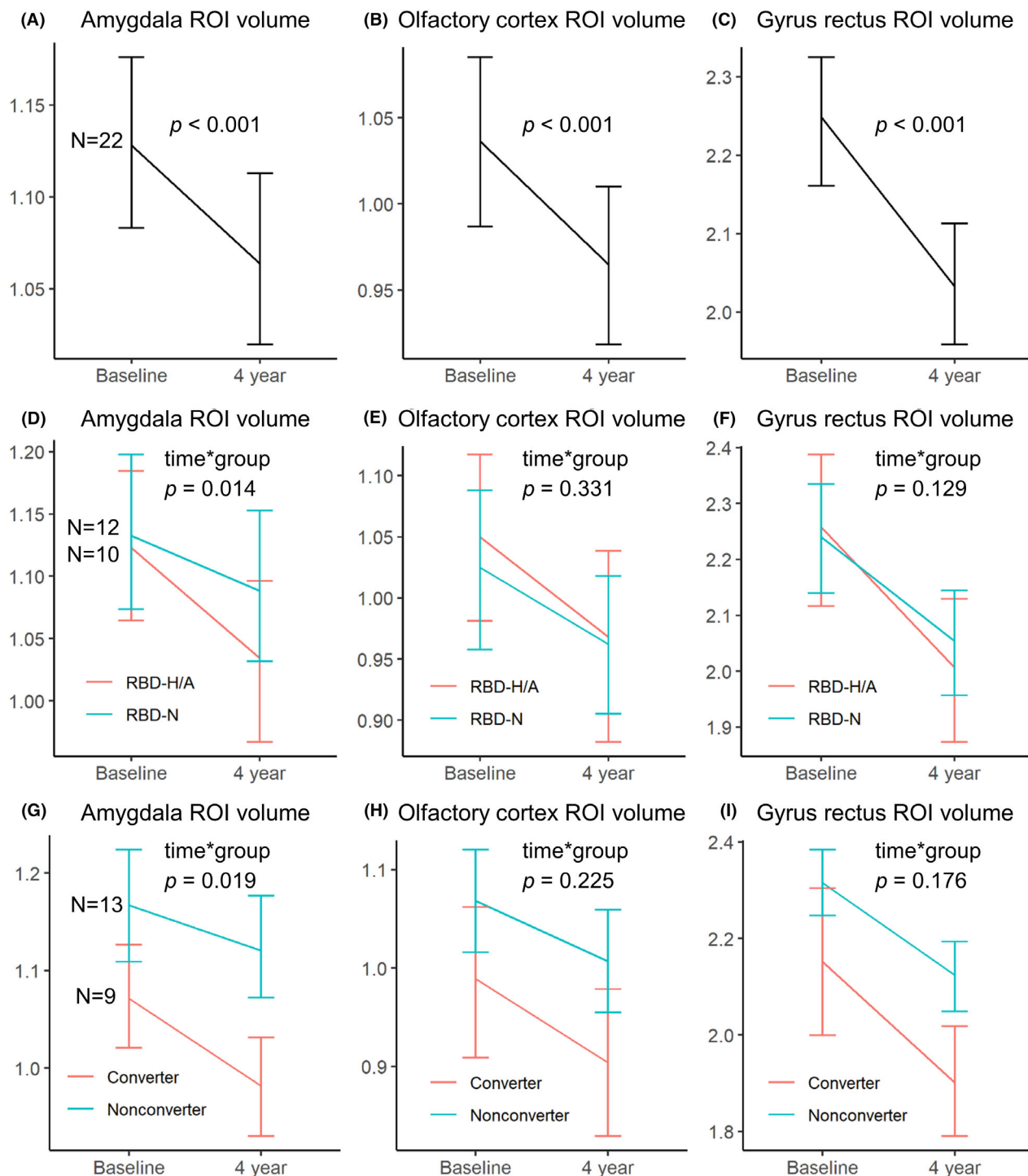
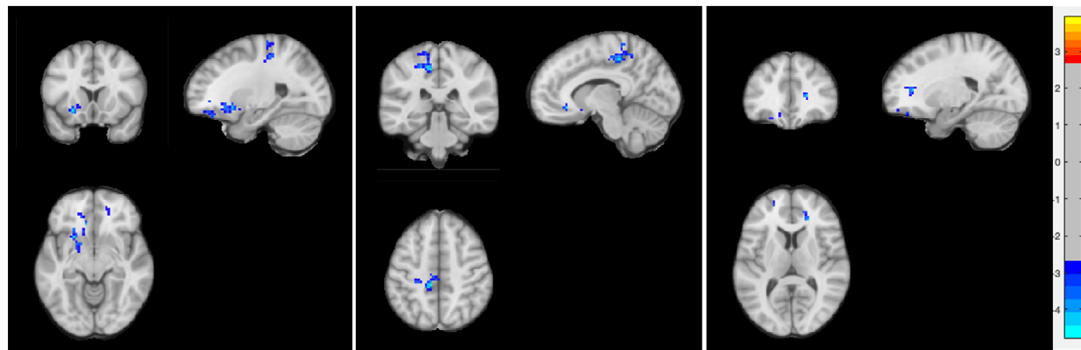
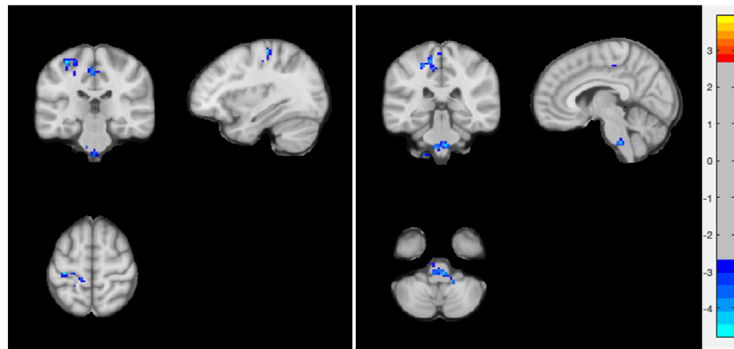


Figure 4. Progression of olfactory-related brain atrophy over 4 years in patients with iRBD. (A–C) Progression of atrophy in the olfactory cortex, gyrus rectus, and amygdala in 22 patients with iRBD who underwent repeated brain volumetric MRI after 4 years, and comparison of subgroups stratified by (D–F) the presence of baseline olfactory dysfunction and (G–I) phenoconversion within the follow-up period. The atrophy of the amygdala was significantly faster in the subgroups of iRBD patients with olfactory dysfunction (RBD-H/A) and phenoconverters. RBD-H/A, RBD-hyposmia/anosmia; RBD-N, RBD-normosmia; ROI, region of interest.

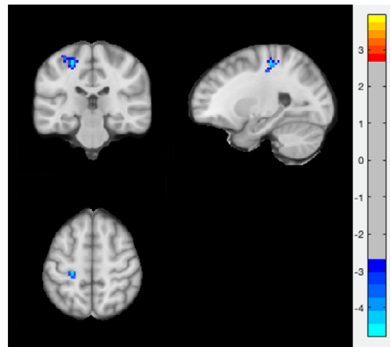
(A) rOLF, iRBD < Controls



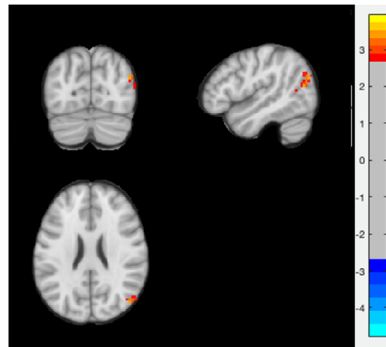
(B) IOLF, iRBD < Controls



(C) IAMYG, iRBD < Controls



(D) IREC, iRBD > Controls



(E) Cluster-specific functional connectivity z values and MPS

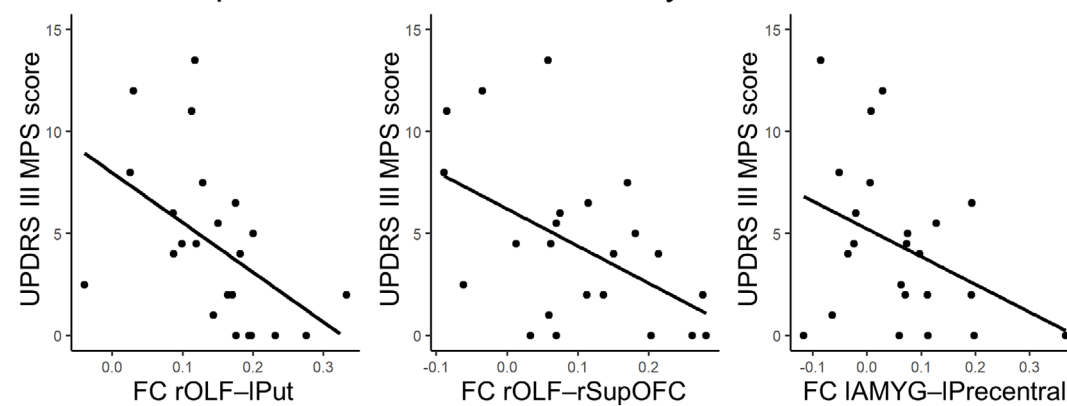


Figure 5. Patients with iRBD exhibit multiple gray matter clusters of aberrant olfactory-related functional connectivity networks. Contrast maps display clusters demonstrating altered functional connectivity with the (A) right and (B) left olfactory cortex, (C) left amygdala, and (D) left gyrus rectus in the iRBD group compared to healthy controls. Thresholds for significance were set at voxel-level $p < 0.01$ and cluster-level $p < 0.05$ (two-sample t -test, two-tailed), corrected for multiple comparisons using the Gaussian random field (GRF) theory correction criteria. The color bars represent corresponding z -values. (E) Partial correlation analysis between subject-specific MPS scores and cluster-specific olfactory-related functional connectivity z -values of the left putamen/superior orbitofrontal cortex (peak coordinates $-24, 15, -9$), right superior orbitofrontal cortex ($9, 21, 36$), and left precentral gyrus (peak coordinates $-24, -27, 54$) clusters in the iRBD group, controlled for age and sex, and FDR-adjusted for multiple comparison of clusters. AMYG, amygdala; FC, functional connectivity; FDR, false discovery rate; OLF, olfactory cortex; MPS, mild parkinsonian signs; Precentral, precentral gyrus; Put, putamen; r/l, right/left; REC, gyrus rectus; SupOFC, superior orbitofrontal cortex; UPDRS, (Movement Disorders Society-) Unified Parkinson's Disease Rating Scale.

of each cluster, including the peak coordinates, is provided in Table S4.

An exploratory partial correlation analysis of the connectivity z -values of each cluster revealed that patients' MPS scores were negatively correlated with the connectivity of the right olfactory cortex with the contralateral putamen (peak coordinates: $-24\ 15\ -9$; Fig. 5E) and the ipsilateral superior orbitofrontal cortex (peak coordinates: $21\ 36\ 9$) clusters. Furthermore, the connectivity of the left amygdala to the ipsilateral precentral gyrus cluster (peak coordinates: $-24\ -27\ 54$) was negatively correlated with MPS scores. No clinical correlation was found in the cluster with increased connectivity with the left gyrus rectus.

Four-year longitudinal changes in olfactory-related functional connectivity

Among the 23 patients, 16 underwent repeated resting-state fMRI after 4 years. Five of these patients developed synucleinopathy, including one PD and four DLB, with three of them (one PD and two DLB) converting within the 4 years. These patients exhibited significant progression of atrophy in the olfactory cortex (mean volume reduction 6.08%), gyrus rectus (9.38%), and amygdala (5.42%) over the 4 years ($p < 0.001$).

In the exploratory comparison analysis of baseline fMRI between these patients and controls (Fig. S5 and Table S5), consistent trends of aberrant olfactory cortex- and gyrus rectus-related functional connectivity in iRBD were observed: Clusters with decreased connectivity to the olfactory cortex were found across the middle cingulate cortex, precentral gyrus, and paracentral lobule, and clusters of increased gyrus rectus connectivity were found in the superior frontal cortex and precuneus. However, in relation to the amygdala, only one cluster with increased connectivity between the right amygdala and cerebellum was identified.

In the exploratory longitudinal comparison of baseline and four-year fMRI pairs in these patients, multiple clusters of increased olfactory cortical connectivity compared to baseline were identified (Fig. S6 and Table S6). The

significant clusters involved the bilateral middle occipital/temporal cortices, bilateral inferior frontal cortices, and right thalamus for the right olfactory cortex as the seed. For the left olfactory cortex as the seed, the clusters included the cerebellum, right thalamus, right middle temporal/occipital cortex, left paracentral lobule, and left middle frontal cortex. Increased functional connectivity with the right and left amygdala was detected in the left lingual gyrus and right inferior frontal cortex, respectively, while connectivity with the left gyrus rectus was reduced in the left fusiform gyrus compared to baseline.

Discussion

In this prospective cohort of iRBD, significant atrophy and functional connectivity changes were identified in brain olfactory-related structures, particularly the olfactory cortex, gyrus rectus, and amygdala. Using a longitudinal dataset, we demonstrate that olfactory-related atrophy progresses over time in iRBD, correlates with prodromal parkinsonian nonmotor features, and is closely associated with an increased risk of phenoconversion. These findings suggest that atrophy of central olfactory structures serves as a potential indicator of premotor synucleinopathy, especially LBDs, in iRBD.

Our VBM findings of olfactory-related atrophy in iRBD align with pathological reports in incidental LBD and PD. An autopsy series of 10 PD, 7 iLBD, and 5 controls revealed α -synuclein pathology across all subregions of the primary olfactory cortex in the PD and iLBD cases.⁶ Harding et al.⁵ observed persistent neuronal loss and Lewy body accumulation in the cortical nuclei of the amygdala, a part of the primary olfactory cortex with major olfactory connections, in postmortem PD cases. While pathological evidence is lacking in iRBD, imaging studies have detected relevant structural changes. A DTI study of 12 iRBD patients and 12 controls demonstrated fractional anisotropy increases in bilateral olfactory regions of iRBD patients.¹³ Additionally, the gyrus rectus was reported to exhibit cortical thinning in 24 iRBD patients compared to 42 controls.³² Our study, for the

first time in a longitudinal cohort of iRBD, demonstrates the progression of olfactory-related brain atrophy in prodromal LBD and its clinical correlates.

Growing evidence suggests that Lewy pathology may progress from the olfactory bulb to central olfactory structures in the early stages. Anatomically, the axons of mitral and tufted cells in the olfactory bulb form the olfactory peduncle, which further constitutes the medial and lateral olfactory striae.³³ The striae extend to the anterior olfactory nucleus and connect to various subregions of the olfactory cortex, including the olfactory tubercle, temporal piriform, and olfactory entorhinal cortices, as well as the cortical nucleus of the amygdala and the cortex–amygdala transition zone (CxA).³³ The gyrus rectus, separated from the orbitofrontal cortex by the olfactory sulcus, also features strong connectivity with the piriform cortex.³⁴ Experimental studies that injected human- and recombinant mouse- α -synuclein preformed fibrils into olfactory bulbs of wild-type mice showed patterns of initial propagation into the piriform and the entorhinal cortices, the cortical amygdaloid nuclei, and the basolateral amygdala within the first month.^{14,17} In contrast, when pathologic α -synuclein preformed fibrils were injected into the gut of mice, the olfactory system was affected later than the substantia nigra.³⁵ A pathological study of 328 postmortem individuals found that α -synucleinopathy in the olfactory bulb predicted the presence of brain LBDs, and the density of synucleinopathy in the bulb most strongly correlated with that in the amygdala compared to other regions such as the substantia nigra or locus coeruleus.³⁶ Our data demonstrate the predictive value of olfactory-related atrophy for future phenotypic conversion in iRBD patients who do not exhibit parkinsonism or dementia at baseline. The results support the hypothesis that Lewy pathology can propagate along the olfactory pathway in early prodromal stages. This might occur independently of gut–brain propagation, which should be further investigated in subsequent studies.

Anxiety and depression, preclinical markers of PD,^{9,37} tended to be associated with olfactory-related atrophy, which is also supported by rodent model and human imaging studies. Injection of α -syn preformed fibrils into the olfactory bulbs of human α -syn transgenic mice resulted in severe α -synuclein pathology accompanied by atrophy along the olfactory pathway, the basolateral amygdala (BLA), and later in the limbic system.¹⁶ Subsequent behavioral analyses revealed hyposmia followed by anxiety-like behavior, suggesting a possible causal relationship between olfactory-related structural alteration and anxiety in prodromal synucleinopathy.¹⁶ The prevalence of depression and anxiety ranges from 25.6% to 28.8%, and 17.7% to 22.6%, respectively, in the human

iRBD population,¹⁰ and probable RBD is associated with greater depression in early PD.³⁸ Volumetric analyses in iRBD and PD reported associations between smaller amygdala volume and greater anxiety.^{39,40} Depressed PD patients also exhibit density alterations in the bilateral gyrus rectus compared to nondepressed PD.⁴¹

The amygdala's involvement in RBD symptoms is also worth considering. During REM dreaming, the limbic and paralimbic areas are selectively activated, which is thought to contribute to the emotional intensity and social nature of dreams.⁴² Among these activated limbic structures is the amygdala, which plays a role in mediating anxiety, a prevalent emotion in dreams.⁴³ Additionally, the collaboration between the amygdala and the hippocampus in storing emotional memories during wakefulness suggests that the reactivation of these areas in REM sleep may contribute to the retrieval of emotionally salient memory.⁴⁴ Considering these findings, it is plausible that changes in the amygdala may contribute to the manifestation of RBD symptoms, specifically through the experience of emotionally charged dreams.

The relationship between amygdala atrophy, dopaminergic denervation, and nonmotor features including olfactory dysfunction in this iRBD cohort is intriguing. Evidence suggests that the amygdala is involved in the initiation of REM sleep itself.⁴⁵ Stimulation of dopaminergic projections from the ventral tegmental area (VTA) and the subsequent increase in dopamine in the BLA inhibit the D2-receptor (DRD2) expressing BLA neurons, leading to a rapid transition to REM sleep.⁴⁵ The DRD2-expressing BLA neurons impact REM motor control by activating GABAergic central amygdala neurons that suppress the key pontine cell groups.^{45,46} While iRBD in prodromal Lewy body disorders has traditionally been associated with lower brainstem pathology, these findings shed new light on the role of dopaminergic signaling disturbances in the amygdala. The BLA is also extensively involved in olfactory processing: It receives dense projections from the CxA, which directly receives inputs from the olfactory bulb,⁴⁷ and has strong reciprocal connections with the posterior piriform cortex.⁴⁸ The central nucleus of amygdala, which receives abundant information from the basolateral complex, has rich connections with autonomic centers.⁴⁹ In this context, the co-occurrence of iRBD, olfactory dysfunction, and autonomic dysfunction in prodromal LBDs may be at least partially explained by a shared anatomical mechanism involving the amygdala. Our study demonstrates that dopaminergic denervation of the amygdala tends to be more pronounced in iRBD patients with olfactory dysfunction (iRBD-H/A) compared to controls, correlates with urinary problems, and that progression of amygdala atrophy is also faster in iRBD-H/A and phenoconverters

than the RBD-normosmia group (iRBD-N) and nonconverters. These findings support the possibility that structural and functional changes in the brain regions associated with the amygdala may play a crucial role in the development of iRBD in prodromal LBDs.

Our data also reveal aberrant functional connectivity between the olfactory cortex and multiple gray matter clusters in iRBD. These changes correlate with subtle motor impairments that precede overt parkinsonism, suggesting that these olfactory-associated alterations in iRBD are indeed linked to the pathophysiology of synucleinopathy, not a product of chance or aging. To our knowledge, this study is the first to present resting-state functional connectivity data using olfactory regions as seeds in iRBD, and it is also the first study with longitudinal follow-up. Regarding the trajectory of olfactory cortical connectivity, it is noteworthy that initially, multiple clusters with reduced connectivity compared to controls were observed, followed by the occurrence of new clusters with enhanced connectivity over 4 years. While it should be noted that increases in connectivity over time in this longitudinal sample do not necessarily indicate hyperconnectivity compared to controls, these temporal changes may indicate a functional compensatory response that accompanies or follows a progressive structural neurodegeneration. Additionally, the direction of gyrus rectus-related connectivity changes exhibited an opposite pattern. The brain regions involved in the olfactory pathway may structurally undergo unidirectional atrophy during the evolution of iRBD into LBD, but their individual changes in the brain signaling system are more likely nonparallel, possibly related to the sequential progression of pathology and compensatory responses.

Our study has several limitations. First, since only two iRBD patients converted to MSA, we were unable to compare their characteristics to those of LBD converters. Instead, we provided descriptive medical history and information on olfactory-related atrophy. The second limitation of our study pertains to the small sample size. As a single-center multimodal imaging study, we encountered limitations in terms of the total number of patients included in our analysis. The number of patients included in the fMRI dataset was limited to about half, and the number in the 4-year follow-up was further limited. A larger longitudinal study will provide insights into the evolution of functional network alterations in prodromal LBDs. Additionally, iRBD patients who developed cognitive decline and additional core clinical features of DLB during follow-up, without definite ADL impairment, were classified as DLB converters, as they were considered more likely to have underlying DLB pathology over other MCI syndromes. However, since the clinical significance could be controversial due to the deferral of dementia

documentation based on ADL performance, we also performed a separate survival analysis excluding these DLB converters with MCI ($N = 2$). The Kaplan–Meier curves are shown in Fig. S7; the subgroups of patients with baseline atrophy in the gyrus rectus (log-rank test, $p = 0.0021$) and amygdala ($p = 0.0053$) still exhibited significantly higher rates of phenoconversion than those without baseline atrophy.

Conclusions

In conclusion, we have demonstrated the presence and progression of significant atrophy in brain olfactory-related structures in patients with iRBD, specifically in the olfactory cortex, gyrus rectus, and amygdala. This atrophy is clinically associated with various nonmotor parkinsonian features, accompanied by aberrant brain functional connectivity, and significantly predicts future phenoconversion to overt synucleinopathy, particularly LBDs, in this longitudinal cohort of iRBD. These early structural and functional alterations in iRBD may indicate the propagation of Lewy pathology along the olfactory system during the premotor stages, which should be worth investigated in a larger longitudinal cohort to confirm our findings.

Author Contributions

Study concept and design: J-Y Lee, H Kim, KA Woo. Data acquisition: J-Y Lee, YK Kim, H Kim, EJ Yoon, H Nam, KA Woo. Data analysis and interpretation: J-Y Lee, H Kim, KA Woo. Drafting the manuscript: J-Y Lee, H Kim, KA Woo. Study supervision: J-Y Lee, YK Kim. Critical review of the manuscript: B Jeon, YK Kim, J-Y Lee, JH Shin.

Acknowledgements

None.

Funding Information

This research is supported by the National Research Foundation of Korea (NRF) grant funded by the Ministry of Science and ICT (MSIT) (No. 2022R1A2C4001834) and by the Ministry of Education, Science and Technology (MEST) (NRF-2018R1C1B3008971, NRF-2018R1A5A2025964 and NRF-2020R1I1A1A01054095) in Korea.

Conflict of Interest

The authors report no competing interests relevant to the manuscript.

References

- Braak H, Del Tredici K, Rub U, de Vos RA, Jansen Steur EN, Braak E. Staging of brain pathology related to sporadic Parkinson's disease. *Neurobiol Aging*. 2003;24:197-211.
- Doty RL, Deems DA, Stellar S. Olfactory dysfunction in parkinsonism: a general deficit unrelated to neurologic signs, disease stage, or disease duration. *Neurology*. 1988;38:1237-1244.
- McShane RH, Nagy Z, Esiri MM, et al. Anosmia in dementia is associated with Lewy bodies rather than Alzheimer's pathology. *J Neurol Neurosurg Psychiatry*. 2001;70:739-743.
- Olichney JM, Murphy C, Hofstetter CR, et al. Anosmia is very common in the Lewy body variant of Alzheimer's disease. *J Neurol Neurosurg Psychiatry*. 2005;76:1342-1347.
- Harding AJ, Stimson E, Henderson JM, Halliday GM. Clinical correlates of selective pathology in the amygdala of patients with Parkinson's disease. *Brain*. 2002;125:2431-2445.
- Silveira-Moriyama L, Holton JL, Kingsbury A, et al. Regional differences in the severity of Lewy body pathology across the olfactory cortex. *Neurosci Lett*. 2009;453:77-80.
- Postuma RB, Gagnon JF, Vendette M, Desjardins C, Montplaisir JY. Olfaction and color vision identify impending neurodegeneration in rapid eye movement sleep behavior disorder. *Ann Neurol*. 2011;69:811-818.
- Ponsen MM, Stoffers D, Booi J, van Eck-Smit BL, Wolters E, Berendse HW. Idiopathic hyposmia as a preclinical sign of Parkinson's disease. *Ann Neurol*. 2004;56:173-181.
- Berg D, Postuma RB, Adler CH, et al. MDS research criteria for prodromal Parkinson's disease. *Mov Disord*. 2015;30:1600-1611.
- Postuma RB, Iranzo A, Hu M, et al. Risk and predictors of dementia and parkinsonism in idiopathic REM sleep behaviour disorder: a multicentre study. *Brain*. 2019;142:744-759.
- Arnaldi D, Chincarini A, Hu MT, et al. Dopaminergic imaging and clinical predictors for phenoconversion of REM sleep behaviour disorder. *Brain*. 2021;144:278-287.
- Jennings D, Siderowf A, Stern M, et al. Conversion to Parkinson disease in the PARS hyposmic and dopamine transporter-deficit prodromal cohort. *JAMA Neurol*. 2017;74:933-940.
- Unger MM, Belke M, Menzler K, et al. Diffusion tensor imaging in idiopathic REM sleep behavior disorder reveals microstructural changes in the brainstem, substantia nigra, olfactory region, and other brain regions. *Sleep*. 2010;33:767-773.
- Rey NL, Steiner JA, Maroof N, et al. Widespread transneuronal propagation of alpha-synucleinopathy triggered in olfactory bulb mimics prodromal Parkinson's disease. *J Exp Med*. 2016;213:1759-1778.
- Rey NL, Wesson DW, Brundin P. The olfactory bulb as the entry site for prion-like propagation in neurodegenerative diseases. *Neurobiol Dis*. 2018;109:226-248.
- Uemura N, Ueda J, Yoshihara T, et al. Alpha-synuclein spread from olfactory bulb causes hyposmia, anxiety, and memory loss in BAC-SNCA mice. *Mov Disord*. 2021;36:2036-2047.
- Rey NL, George S, Steiner JA, et al. Spread of aggregates after olfactory bulb injection of alpha-synuclein fibrils is associated with early neuronal loss and is reduced long term. *Acta Neuropathol*. 2018;135:65-83.
- Shin JH, Lee JY, Kim YK, et al. Longitudinal change in dopamine transporter availability in idiopathic REM sleep behavior disorder. *Neurology*. 2020;95:e3081-e3092.
- McKeith IG, Boeve BF, Dickson DW, et al. Diagnosis and management of dementia with Lewy bodies: fourth consensus report of the DLB consortium. *Neurology*. 2017;89:88-100.
- Lee JY, Yoon EJ, Kim YK, et al. Nonmotor and dopamine transporter change in REM sleep behavior disorder by olfactory impairment. *J Mov Disord*. 2019;12:103-112.
- Yoon EJ, Lee JY, Kim H, et al. Brain metabolism related to mild cognitive impairment and phenoconversion in patients with isolated REM sleep behavior disorder. *Neurology*. 2022;98:e2413-e2424.
- Postuma RB, Lang AE, Gagnon JF, Pelletier A, Montplaisir JY. How does parkinsonism start? Prodromal parkinsonism motor changes in idiopathic REM sleep behaviour disorder. *Brain*. 2012;135:1860-1870.
- Goetz CG, Stebbins GT, Tilley BC. Calibration of unified Parkinson's disease rating scale scores to Movement Disorder Society-unified Parkinson's disease rating scale scores. *Mov Disord*. 2012;27:1239-1242.
- Ha JG, Kim J, Nam JS, et al. Development of a Korean culture-friendly olfactory function test and optimization of a diagnostic cutoff value. *Clin Exp Otorhinolaryngol*. 2020;13:274-284.
- Shin C, Lee JY, Kim YK, et al. Cognitive decline in association with hyposmia in idiopathic rapid eye movement sleep behavior disorder: a prospective 2-year follow-up study. *Eur J Neurol*. 2019;26:1417-1420.
- Litvan I, Goldman JG, Troster AI, et al. Diagnostic criteria for mild cognitive impairment in Parkinson's disease: Movement Disorder Society Task Force guidelines. *Mov Disord*. 2012;27:349-356.
- Tzourio-Mazoyer N, Landeau B, Papathanassiou D, et al. Automated anatomical labeling of activations in SPM using a macroscopic anatomical parcellation of the MNI MRI single-subject brain. *Neuroimage*. 2002;15:273-289.

28. Rolls ET, Huang CC, Lin CP, Feng J, Joliot M. Automated anatomical labelling atlas 3. *Neuroimage*. 2020;206:116189.
29. Postuma RB, Berg D, Stern M, et al. MDS clinical diagnostic criteria for Parkinson's disease. *Mov Disord*. 2015;30:1591-1601.
30. Benjamini Y, Hochberg Y. Controlling the false discovery rate—a practical and powerful approach to multiple testing. *J R Stat Soc B*. 1995;57:289-300.
31. Wenning GK, Stankovic I, Vignatelli L, et al. The Movement Disorder Society criteria for the diagnosis of multiple system atrophy. *Mov Disord*. 2022;37:1131-1148.
32. Rahayel S, Montplaisir J, Monchi O, et al. Patterns of cortical thinning in idiopathic rapid eye movement sleep behavior disorder. *Mov Disord*. 2015;30:680-687.
33. Ubeda-Banon I, Saiz-Sanchez D, Flores-Cuadrado A, et al. The human olfactory system in two proteinopathies: Alzheimer's and Parkinson's diseases. *Transl Neurodegener*. 2020;9:22.
34. Fjaeldstad A, Fernandes HM, Van Hartevelt TJ, et al. Brain fingerprints of olfaction: a novel structural method for assessing olfactory cortical networks in health and disease. *Sci Rep*. 2017;7:42534.
35. Kim S, Kwon SH, Kam TI, et al. Transneuronal propagation of pathologic alpha-synuclein from the gut to the brain models Parkinson's disease. *Neuron*. 2019;103:627-641.e7.
36. Beach TG, White CL 3rd, Hladik CL, et al. Olfactory bulb alpha-synucleinopathy has high specificity and sensitivity for Lewy body disorders. *Acta Neuropathol*. 2009;117:169-174.
37. Chaudhuri KR, Healy DG, Schapira AH, National Institute for Clinical Excellence. Non-motor symptoms of Parkinson's disease: diagnosis and management. *Lancet Neurol*. 2006;5:235-245.
38. Rolinski M, Szezyk-Krolkowski K, Tomlinson PR, et al. REM sleep behaviour disorder is associated with worse quality of life and other non-motor features in early Parkinson's disease. *J Neurol Neurosurg Psychiatry*. 2014;85:560-566.
39. Bourgouin PA, Rahayel S, Gaubert M, et al. Gray matter substrates of depressive and anxiety symptoms in idiopathic REM sleep behavior disorder. *Parkinsonism Relat Disord*. 2019;62:163-170.
40. Vriend C, Boedhoe PS, Rutten S, Berendse HW, van der Werf YD, van den Heuvel OA. A smaller amygdala is associated with anxiety in Parkinson's disease: a combined FreeSurfer-VBM study. *J Neurol Neurosurg Psychiatry*. 2016;87:493-500.
41. Feldmann A, Illes Z, Kosztolanyi P, et al. Morphometric changes of gray matter in Parkinson's disease with depression: a voxel-based morphometry study. *Mov Disord*. 2008;23:42-46.
42. Braun AR, Balkin TJ, Wesenten NJ, et al. Regional cerebral blood flow throughout the sleep-wake cycle. An H2(15)O PET study. *Brain*. 1997;120(Pt 7):1173-1197.
43. Hobson JA, Pace-Schott EF, Stickgold R. Dreaming and the brain: toward a cognitive neuroscience of conscious states. *Behav Brain Sci*. 2000;23:793-842. discussion 904-1121.
44. Hobson JA, Pace-Schott EF. The cognitive neuroscience of sleep: neuronal systems, consciousness and learning. *Nat Rev Neurosci*. 2002;3:679-693.
45. Hasegawa E, Miyasaka A, Sakurai K, Cherasse Y, Li Y, Sakurai T. Rapid eye movement sleep is initiated by basolateral amygdala dopamine signaling in mice. *Science*. 2022;375:994-1000.
46. Arrigoni E, Fuller PM. Addicted to dreaming. *Science*. 2022;375:972-973.
47. East BS, Fleming G, Vervoordt S, Shah P, Sullivan RM, Wilson DA. Basolateral amygdala to posterior piriform cortex connectivity ensures precision in learned odor threat. *Sci Rep*. 2021;11:21746.
48. Cadiz-Moretti B, Abellan-Alvaro M, Pardo-Bellver C, Martinez-Garcia F, Lanuza E. Afferent and efferent connections of the cortex-amygdala transition zone in mice. *Front Neuroanat*. 2016;10:125.
49. Braak H, Braak E, Yilmazer D, et al. Amygdala pathology in Parkinson's disease. *Acta Neuropathol*. 1994;88:493-500.

Supporting Information

Additional supporting information may be found online in the Supporting Information section at the end of the article.

Figure S1. Participant flow of four-year follow-up 3T volumetric MRI and resting-state functional MRI.

Figure S2. Comparison of baseline olfactory-related ROI volumes and amygdala ¹⁸F-FP-CIT uptake between healthy controls and iRBD subgroups stratified by the presence of mild parkinsonian sign and olfactory dysfunction.

Figure S3. Forest plot of combined Cox regression analysis model including olfactory cortex atrophy and hyposmia.

Figure S4. Kaplan-Meier curves showing disease-free survival in patients with iRBD, excluding two MSA converters.

Figure S5. Clusters of aberrant olfactory-related functional connectivity at baseline compared to controls, in the 16 iRBD patients who scanned resting-state fMRI four years later.

Figure S6. Four-year longitudinal changes of olfactory-related functional connectivity in 16 iRBD patients.

Figure S7. Kaplan-Meier curves showing disease-free survival in patients with iRBD, excluding two DLB converters with MCI.

Table S1. Brain regions showing significant changes of gray matter volume between iRBD and healthy controls.

Table S2. Cox regression analysis for each baseline predictor of phenoconversion in the longitudinal cohort of iRBD.

Table S3. Cox regression analysis for each baseline predictor of phenoconversion in the longitudinal cohort of iRBD, excluding MSA converter.

Table S4. Clusters with aberrant functional connectivity in patients with iRBD compared to healthy controls.

Table S5. Clusters of aberrant olfactory-related functional connectivity at baseline compared to controls, in the 16 iRBD patients who underwent resting-state fMRI four years later.

Table S6. Clusters showing altered functional connectivity at four-year follow-up fMRI compared to baseline fMRI in 16 iRBD patients.